The Implementation of Numerical Codes for the Analysis of Solar Flux Inputs and the Optimization of Thermal Comfort for a Monobloc Habitat

Abdellatif Oudrane[1,*], Benaoumeur Aour[1] and Messaoud Hamouda[2]

[1]*Laboratory of Applied Biomechanics And Biomaterials (LABAB), BP 1523 El Mnaour, National Polytechnic School of Oran-Maurice Audin (ENPO-MA), 31000, Oran, Algeria*
[2]*Laboratory of Sustainable Development and Informatics (LDDI), Faculty of Science and Technology, Ahmed Draya University of Adrar, Algeria*
E-mail: abdellatif.habadat@gmail.com; ben_aour@yahoo.fr; jhamouda@yahoo.fr
[*]*Corresponding Author*

Received 28 October 2021; Accepted 04 May 2022;
Publication 27 June 2022

Abstract

The purpose of this work is to design computer codes to estimate the different thermal exchanges of the facades of a habitable envelope with its environment in order to optimize thermal comfort. This optimization is based on the use of real climate data from the region under consideration. To achieve this goal, we have developed five fundamental codes in FORTRAN language. The first code consists in Modelling the flow of the heat transfer fluid in the heating slab pipe. The second is designed to model the heat transfer by conduction within the concrete slab. The third is developed for the Modelling of thermal exchanges in a habitable envelope assimilated to a parallelepipedal cavity based on the nodal method. The fourth code is reserved for the Modelling of solar radiation by evaluating the wage flux density on different positions of the walls. The fifth and last code is dedicated to the evaluation of the perfect

European Journal of Computational Mechanics, Vol. 31_2, 155–196.
doi: 10.13052/ejcm2642-2085.3121

thermal coupling between the concrete slab and the heat transfer fluid pipes. The validation of the models implemented in the calculation codes was made on the basis of data measured recently for a clear sky of solar radiation at the radiometric station of the renewable energies research unit in the Saharan environment URER'MS of Adrar. The results obtained showed a very good agreement between the calculated values using the computational codes developed and those measured by the radiometric station of the URER'MS during the typical day.

Keywords: Saharan environment, computational codes, radiometric station, solar radiation, thermal exchange, thermal coupling.

List of Symbols

Nomenclature

a	Width of the wall	m
A	Considered exchange area	m^2
b	Height of the wall	m
c	Length of the wall.	m
Cp	Specific heat of the fluid	$kJ.Kg^{-1}.K^{-1}$
d	Tube diameter	m
e	Wall thickness	m
Gr	Dimensionless Grashof number	$-$
$\overline{H_0}$	Monthly average of daily amounts of solar radiation	$W.m^{-2}$
H_0	Daily sum of extra-terrestrial solar radiation	$W.m^{-2}$
h	Height of the sun	$(^\circ)$
h_s	Sunrise time	h
Nu	Dimensionless Nusselt number	$-$
I_0	Solar illumination at the atmosphere top	$W.h.m^{-2}$
K	Wall conduction coefficient	$W.m^{-1}.K^{-1}$
P	Heat transfer fluid pressure	Pa
Q_{abs}	Amount of heat absorbed	$W.m^{-2}$
Q_{emis}	Amount of heat emitted	$W.m^{-2}$
φ	Latitude of the location	$(^\circ)$
ϕ_i	Amount of elementary heat emited	W
R	Thermal resistance of the wall	$m^2.K.W^{-1}$
t	Time	s
t_G	Overall calculation time	s

T	Temperature	*(°C)*
T_b	Temperature of the concrete slab	*(°C)*
T_f	Fluid temperature	*(°C)*
$\mathrm{T_{amb}}$	Ambient temperature	*(°C)*
L	Slab length in	*(m)*
U	Fluid velocity along the (Ox) axis	$m.s^{-1}$
V	Fluid velocity along the (Oy) axis	$m.s^{-1}$
ZM	Sun azimuth	*(°)*

Greek letters

α_i	Absorption coefficient of the material	–
δ	Phase shift time between maximum temperature and maximum radiation	*h*
λ	Thermal conductivity of the fluid	$W.m^{-1}.K^{-1}$
λ_b	Thermal conductivity of concrete	$W.m^{-1}.K^{-1}$
λ_f	Thermal conductivity of the fluid	$W.m^{-1}.K^{-1}$
Cp_b	Concrete heat capacity	$kJ.Kg^{-1}.K^{-1}$
Γ	Nebulosity	–
θ_{PS}	Inclination angle of the south wall	*(°)*
θ_{PN}	Inclination angle of the north wall	*(°)*
θ_{PO}	Inclination angle of the nest wall	*(°)*
θ_{PE}	Inclination angle of the east wall	*(°)*
θ_{PFP}	Inclination angle of the wall bottom ceiling	*(°)*
ρ	Density of the fluid	$Kg.m^{-3}$
ρ_b	Density of the concrete	$Kg.m^{-3}$
Λ	Sunshine duration	*h*
ω	Hourly sun angle	*(°)*
ω_s	Hourly sunrise angle for a horizontal plane	*(°)*

Abbreviations

GSF	Global solar flux	$W.m^{-2}$
GHSF	Global horizontal solar flux	$W.m^{-2}$
ISFS	Incident solar flux on the South wall	$W.m^{-2}$
ISFW	Incident solar flux on the West wall	$W.m^{-2}$
ISFE	Incident solar flux on the East wall	$W.m^{-2}$
HDIFR	Horizontal diffuse radiation	$W.m^{-2}$
HDIRR	Horizontal direct radiation	$W.m^{-2}$
GRIN	Global radiation incident on the North wall	$W.m^{-2}$
GRIS	Global radiation incident on the South wall	$W.m^{-2}$

GRIW	Global radiation incident on the West wall	$W.m^{-2}$
GRIE	Global radiation incident on the East wall	$W.m^{-2}$
URER'MS	Research Unit of Renewable Energies in Saharan Medium	–
TEFE	Temperature of the external facade of the East wall	$(^{\circ}C)$
TEFCS	Temperature of the external facade of the Ceiling slab	$(^{\circ}C)$
TEFN	Temperature of the external facade of the North wall	$(^{\circ}C)$
TEFS	Temperature of the external facade of the South wall	$(^{\circ}C)$
TEFW	Temperature of the external facade of the West wall	$(^{\circ}C)$
TIFN	Temperature of the internal facade of the North wall	$(^{\circ}C)$
TIFS	Temperature of the internal facade of the South wall	$(^{\circ}C)$
TIFCS	Temperature of the internal facade of the Ceiling slab	$(^{\circ}C)$
TIFW	Temperature of the internal facade of the West wall	$(^{\circ}C)$
TIFE	Temperature of the internal facade of the East wall	$(^{\circ}C)$
ND	Number of days elapsed since January 1st	–

1 Introduction

The sun is the main source of energy available on Earth. This includes direct thermal energy. Knowledge of the position of the sun in the sky at anytime and anywhere is necessary for the study of intercepted energy. The times of sunrise and sunset, as well as the sun path in the sky during a day, allow us to assess quantities, such as the maximum duration of insolation, the solar flux and the ambient temperature [1].

Solar energy is used in different ways, either in photovoltaic systems for the electricity production or in thermal systems (solar water heaters) for the hot water production, a field in which it is experiencing considerable development, particularly in the habitat sector [2].

Zarai et al. [3] presented the design of a sizing and planning code for the production of a solar thermal installation by making an estimate of the evolution of the global solar flux and ambient temperature during a daytime. All results are visualized through graphical interface designed using Matlab software.

Zhipeng et al. [4] have developed a model for the estimation of clear sky illuminance based on work carried out within the framework of a European project, leading to a computer version that can be run in an operational manner, by estimating the uncertainties of the radiation in its different components (direct and diffuse).

The development of buildings contributes mainly to the challenges of the energy transition to better reduce its consumption, ensure better comfort, meet environmental and regulatory requirements, while minimizing the total price. Abbass et al. [5] proposed a numerical tool design from the sketch phase to the more advanced design phase. This numerical tool is based on solutions offering a global vision of the building and allowing to make optimal choices using the internet, to cover the aspects of global Modelling and decision support.

Arantes et al. [6] presented an optimization methodology using genetic algorithms for Modelling the morphogenesis of a city region with respect to three criteria (energy, density and direct sunlight). The purpose of this methodology is to discuss the interests and limitations of such a micro-urban morphogenesis method.

Dinh et al. [7] presented an optimal sizing methodology integrating the management strategy of a complex energy system (heating, air conditioning, PV and electrochemical storage) for a building connected to the network. They approved that the thermal comfort is determined through a reduced order dynamic thermal envelope model, and life-cycle cost is taken into account as optimization criteria while load coverage is considered as one of the constraints.

Jean et al. [8] presented a numerical model to simulate the thermo-hydro-hygric behavior of complex vegetated walls (CVW). They deduced a system of physical description allowing the Modelling of CVW by coupling the observed fields.

Oudrane et al. [9] have established an adequate methodology to properly dimension and optimize the geometric and thermal parameters of the solar system (PSD). The latter has been implemented in a computational code in order to automate the optimization procedure.

In this context, the objective of this paper is to develop computer tools to model and optimize thermal comfort in a habitat. It is important to note that such tools can be used by architects and design offices for the prediction of the habitat energy behavior and its adequacy with current standards.

To achieve this objective, we started with a presentation of the mathematical formulation. Section 3 was reserved for a general description of the developed computational codes. The method of resolution and the physical model studied are presented respectively in Sections 4 and 5. Section 6 was reserved for the interpretation of the climatic data of the typical day. The 7th section was devoted to the presentation of the results and discussion. A conclusion on the obtained results is presented at the end of this work.

2 Mathematical Modelling

2.1 Fluid Flow Modelling

2.1.1 Simplifying hypotheses

In order to simplify the mathematical modelling of fluid flow, a set of hypotheses is assumed for this study. These assumptions are derived from the physical properties of fluid flow in a horizontal pipe embedded in a concrete slab and are summarized as follows:

- The fluid is Newtonian, viscous and incompressible;
- The flow is transient with a laminar regime;
- The viscous dissipation is negligible: since the speed and the viscosity of water are low;
- The flow has only two velocity components: longitudinal and transversal;
- No internal sources of heat $\phi_s = 0$;
- The physical properties (μ, C_p, ρ, λ) are constant;
- The low thickness of the pipe is neglected in numerical calculations;
- The fluid-structure interface is in thermodynamic equilibrium;
- The solid medium is isotropic.

2.1.2 Mathematical model

Firstly, we opted for a flow study in a pipe of rectangular cross-section. It is a viscous fluid flow between two parallel large plates separated by a small distance d. Both plates are fixed and the fluid is set in motion by a pressure gradient (Figure 1). The solution governing a Poiseuille flow of maximum velocity, U_0, at the pipe middle is given by [10]:

$$U(y) = U_0 \cdot \left(1 - 4\left(\frac{y}{d}\right)^2\right) \tag{1}$$

A rigorous treatment of the boundary layer would require the complete solution of Navier-Stokes equations. Their complexity prompted Prandtl to simplify them by retaining only the most important terms. The main idea is to neglect the axial gradients (∂/∂x) in front of the transverse gradients (∂/∂y). Thus, we obtain the Prandtl equations for the boundary layer which govern the laminar flow in the heating slab pipe as follows [11–13]:

- ***Equation of Momentum***

$$\frac{\partial u}{\partial t} + u\frac{\partial u}{\partial x} + v\frac{\partial u}{\partial y} = -\frac{1}{\rho}\frac{\partial P}{\partial x} + v\frac{\partial^2 u}{\partial y^2} \quad \textit{and} \quad \frac{\partial P}{\partial y} = 0 \tag{2}$$

Figure 1 Description of fluid flow in the concrete slab pipe.

- ***Equation of Mass Conservation***

$$\frac{\partial u}{\partial x} + \frac{\partial v}{\partial y} = 0 \tag{3}$$

- ***Equation of Energy Conservation***

$$\frac{\partial T}{\partial t} + u\frac{\partial T}{\partial x} + v\frac{\partial T}{\partial y} = \frac{\lambda}{\rho \cdot C_p}\frac{\partial^2 T}{\partial y^2} \tag{4}$$

2.1.3 Resolution method

The Navier-Stokes equations that govern this flow have been solved numerically using an implicit finite difference method. The systems of algebraic equations thus obtained have been solved by the Gauss and Thomas algorithms.

2.2 Thermal Diffusion Modelling

2.2.1 Mathematical model

The floor slab is considered as a homogeneous solid on which the classical equation of heat diffusion is applied [14]. Heat diffusion is defined as the mode of heat transfer in a solid caused by a temperature difference between two regions of this solid medium. The numerical modelling is based on two-dimensional study of heat conduction within the heating slab. The thermal conduction equation is given by [15, 16]:

$$\frac{\partial T_b}{\partial t} = \frac{\lambda_b}{\rho_b \cdot Cp_b} \cdot \left(\frac{\partial^2 T_b}{\partial x^2} + \frac{\partial^2 T_b}{\partial y^2}\right) \tag{5}$$

2.2.2 Initial and boundary conditions

The slab is assumed initially in the ambient temperature at 25°C, then a constant temperature gradient is applied. This gradient causes a temperature difference between the atmosphere and the concrete slab. This means that the temperature $T_b\ (x, y, t)$ at time $(t = 0s)$ is zero:

$$T_b(x, y, 0) = 0.0 \quad \forall\, x \quad \textit{and} \quad \forall\, y \tag{6}$$

Due to the effect that the concrete slab is in contact with the outside environment, the boundary conditions are defined as:

$$\begin{aligned} T_b(x, y, t) &= T_b(0, b, 0) = 0.0 \quad \forall\, y \\ T_b(x, y, t) &= T_b(L, b, 0) = 0.0 \quad \forall\, y \\ T_b(x, y, t) &= T_b(L, b, 0) = T_{amb} \quad \forall\, x \\ T_b(x, y, t) &= T_b(L, 0, 0) = 0.0 \quad \forall\, x \end{aligned} \tag{7}$$

2.2.3 Resolution method

The governing thermal diffusion equation is discretized by an implicit finite difference method. The system of algebraic equations thus obtained is solved by the Thomas algorithm.

2.3 Modelling of Thermal Coupling

The stationary coupling fluid-structure has been dealt with several times. It consists in coupling the solver of the Navier-Stokes equations to the conduction equations and searching for a stationary state in fluid and structure medium. It should be noted that this type of problem has already been studied numerically by Errera et al. [17]. Although using the same tools, the work presented here is different in nature. Indeed, we are interested in the unsteady coupling and more precisely in the detailed description of the heat exchanges in a concrete slab subjected to a convective flow due to a laminar flow.

2.3.1 Fluid-structure interface

Figure 2 shows the interface that separates two media with different thermal conductivities. The distance between the node *(J)* and the neighboring nodes ($J - 1$ and $K + 1$) is calculated as function of the space step [18–20].

A finite difference formulation based on the Galerkin method has been used to solve the equations that govern the fluid-structure interaction in the heating slab [21]. In a perfect contact, let us consider the case where

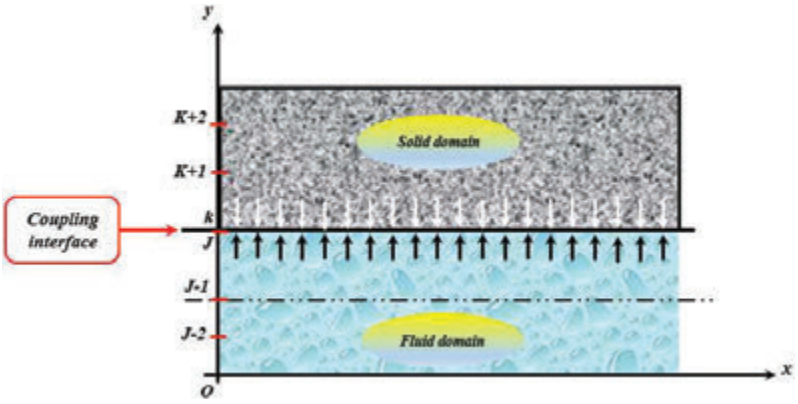

Figure 2 Spatial discretization at the fluid-structure interface.

the parietal transfer is entirely of convecto-conductive nature. Whatever the convection mode, the energy transfer between the solid body surface at the temperature (*Ts*) and the fluid takes place by thermal conduction since the fluid velocity is zero on the solid body surface. The continuity of the energy flow density at the surface allows us to write [22–24]:

$$-\lambda_b \cdot \left.\frac{\partial T_b}{\partial y}\right|_{y=0} = -\lambda_f \cdot \left.\frac{\partial T_f}{\partial y}\right|_{y=0} \tag{8}$$

2.3.2 Resolution method

The discretization of the energy flow density terms at the lower surface of the solid using an implicit finite differences method with a three-point forward scheme is given by:

$$-\lambda_b \cdot \left.\frac{\partial T_b}{\partial y}\right|_{y=0} = \lambda_b \cdot \left[\frac{3 \cdot T_b(I,K) - 4 \cdot T_b(I,K+1) + T_b(I,K+2)}{2\Delta y}\right] \tag{9}$$

On the other hand, the discretization of the energy flow density terms at the upper surface of the fluid using an implicit finite differences method with a three-point rear scheme is given by:

$$-\lambda_f \cdot \left.\frac{\partial T_f}{\partial y}\right|_{y=0} = \lambda_f \cdot \left[\frac{3 \cdot T_f(I,J) + 4 \cdot T_f(I,J-1) - T_f(I,J-2)}{2\Delta y}\right] \tag{10}$$

where:

J: The increment index on the y-axis in the fluid subdomain;
K: The increment index of the y-axis in the concrete subdomain.

2.4 Modelling of Heat Transfer in the Habitable Envelope

2.4.1 Mathematical model

The method adopted to describe the thermodynamic behavior of the habitat model is based on temperature analysis. In general, if we consider a given node (i) of a habitat component, the instantaneous energy change in that component is equal to the algebraic sum of heat flux densities exchanged through that component. It is written as follows [25, 26]:

$$\frac{m_i \cdot Cp_i}{A} \cdot \frac{\partial T_i}{\partial t} = DFS_i + \phi_i + \sum_i \sum_j \phi x_i \quad \textit{and} \quad DFS_i = \alpha_i \cdot \varphi_i \tag{11}$$

2.4.2 Assumptions and methodology

In the building energy field, predictive numerical models have become in a few years a widely used tool [27]. The numerical models in this work have been developed mainly to meet the sizing needs of habitat. These models concern only the thermal exchanges between the external environment and the external facades, and the internal environment with the internal facades taking into account the climatic conditions of the implantation site, which is well detailed in Figure 3. The algebraic equations systems that obtained have been solved by Gaussian algorithms. The proposed mathematical model is based on some assumptions that can be summarized as follows:

- Thermal transfers through the walls are assumed unidirectional and perpendicular to the walls;
- The air velocity inside the habitable envelope is negligible;
- The temperature distribution on the outer and inner surfaces of the walls is uniform;
- Convection is natural with laminar flow;
- The door and the window are supposed to be perfectly closed;
- The moisture is neglected (dry air), depending on the climate of the site in summer;
- The density of the solar flux incident on the different facades of the habitat is calculated by a semi-empirical model;

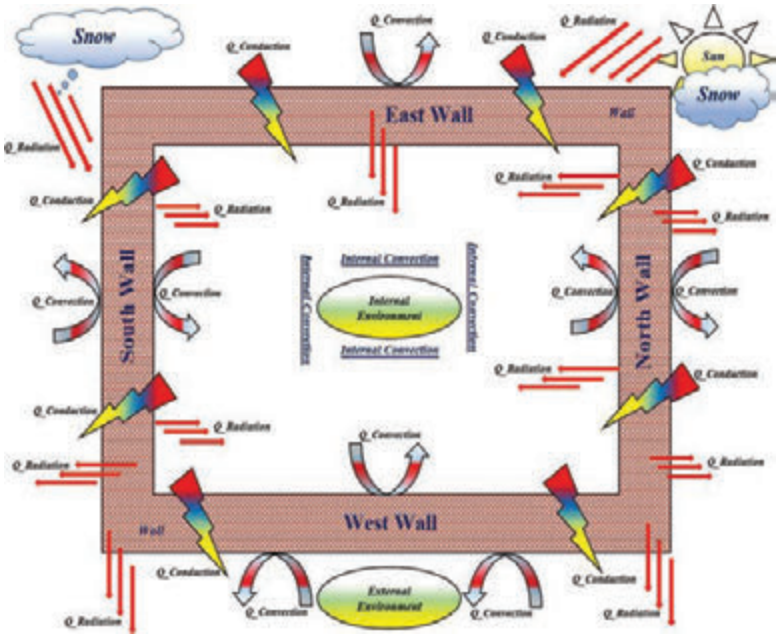

Figure 3 Description of the different modes at heat exchange between the habitable envelope and its surroundings.

- The outside temperature is equal to the floor temperature: $T_{amb} = T_{soil}$;
- The bricks are assumed to be solid and isotropic.

It is important to note that the air stratification of the zone, the wind influence on the infiltrations of air, the water diffusion in the walls and the state changes are not taken into account. Consequently, neither the latent heat storage is treated, nor the effect of the humidity variations. The method followed aims to ensure the mastery of the hypotheses and to develop the modelling aspects associated with the different modes of heat transfer (radiation, convection and conduction). The discretization of the equations systems is done by the finite difference method based on the nodal method to deduce the energy balances of each wall in the habitable envelope.

2.4.3 Heat transfer through the walls

It should be noted that the heat flow transmitted by conduction through a flat wall depends on [28]:

- The wall thickness;
- The nature of the material;

- The temperatures of the inner and outer faces of the wall;
- The conduction coefficient of the wall $k = \lambda/e$. Indeed, the more this coefficient decreases or increases, the less the wall conducts heat, and the more the wall resists the passage of heat, i.e., the more it is insulating.

The thermal resistance of a wall to conduction is given by:

$$R = e/\lambda \Leftrightarrow r = 1/K \tag{12}$$

In the case of a wall composed of several layers of different materials, the conduction resistance of the whole is the sum of all the resistances of each material [29, 30]:

$$R = \sum e/\lambda \tag{13}$$

The roof consists of moulded earth and palm waste. In this case, these are the horizontal surfaces in contact with the habitat. Then the overall thermal resistance of the roof is [29, 30]:

$$R = \frac{1}{h_i} + \frac{1}{h_i} + \frac{e_{\text{sand}}}{\lambda_{\text{sand}}} + \frac{e_{\text{wastes}}}{\lambda_{\text{wastes}}} \tag{14}$$

2.5 Modelling of Solar Radiation

The hourly variations of the global solar flux and the temperature of the external environment of the region under consideration are expressed by means of two periodic functions written in sinusoidal form as follows [31, 32]:

$$FS(t) = FSH_{\max} \times \sin\left[\frac{\pi}{\Lambda} \cdot (h - h_s)\right] \tag{15}$$

$$T_0(t) = \left(\frac{T_{0\max} + T_{0\min}}{2} - \frac{T_{0\max} + T_{0\min}}{2}\right) \times \sin\left(\frac{2 \cdot \pi \cdot h}{\Lambda} - \delta\right) \tag{16}$$

The solar flux captured by the roof was evaluated using the model of Lui and Jordan [33, 34], which considerably reduces the size of the meteorological file and provides results that are not very sensitive to the random distribution of solar radiation in the month. This method leads to the notion of a typical day characteristic of the climate in a given zone. The purpose of the notion of a typical day is to calculate the hourly solar flux captured by an inclined plane knowing the monthly average values of the daily global flux on a horizontal plane [34].

2.5.1 Calculation for a clear sky on a horizontal plane

The global radiation (GHSF) received by a horizontal plane is divided into two terms:

- Direct radiation (HDIRR) (luminance corrected for atmospheric phenomena);
- The diffuse radiation (HDIFR) comes from the whole celestial vault.

Therefore, for a horizontal plane the global radiation is [35, 36]:

$$GHSF = (HDIRR) \times sin(h) + HDIFR = (HDIRR) + HDIFR \quad (17)$$

2.5.2 Calculation of diffuse radiation for a horizontal plane

The diffuse radiation for a horizontal surface is given by the expression [37]:

$$\mathrm{HDIFR} = 120 \cdot \Gamma \cdot \exp\left(\frac{-1}{0,4511 + \sin(h)}\right) \quad \textit{and}$$

$$\Gamma = 0,796 - 0,01 \cdot \sin\left(\frac{360}{365}(ND + 284)\right) \quad (18)$$

where Γ is the nebulosity and *ND* is the number of days elapsed since January 1st.

3 General Description of the Developed Computer Codes

The developed computer codes are programs established for performing thermodynamic simulations of a habitable envelope. We started in the first part by implementing numerical models for Modelling the heat transfer of the hot water flow in the heating slab pipe. For this, we have based on the Navier-Stokes and the heat equations that govern this flow. These equations have been discretized by an implicit finite difference method. The resulting system of algebraic equations was solved using Gauss and Thomas algorithms [38, 39].

Then, in a second phase, we implemented the conduction equation in the concrete slab using the same methodology as for the flow. The heat transfers that take place in a habitat model assimilated to a parallelepiped cavity have been modelled using the thermal balances established at each wall of the habitat and taking into account heat exchanges by convection, conduction and radiation [40].

The calculation in this phase consists in reducing a model to finite differences by modal analysis. Non-linear quantities are introduced in the

simulation phase. This tool has been improved and completed by the generation of hourly weather files of different components of the daily solar flux, files of incident solar flux for each face of the habitable envelope, as well as their external and internal temperatures in each hour of the typical day. Noting that this tool is flexible and accessible to solar thermal researchers.

In order to spread out this description, we have subdivided this computer tool into five fundamental computational codes which have been named as follows:

- **CFD:** Code for the Fluid Dynamics in the slab pipe.
- **CHC:** Code of the Heat Conduction in the slab.
- **CTC:** Code for the fluid-structure Thermal Coupling.
- **CTE:** Code of the Thermal Exchange Modelling in the habitat.
- **CSR:** Code of the Solar Radiation evaluation.

3.1 Description of CFD Code

The CFD code is a program developed for solving the differential equations that govern the mass transport, momentum, laminar variables and energy. In this study, we are interested to the Modelling of the coolant flow, as well as the heat and mass transfer processes in the concrete slab pipe. The calculation steps are detailed by the flowchart presented in Figure 4.

3.2 Description of CHC Code

The CHC code is dedicated to the thermal behavior simulation of the concrete slab under the thermal diffusion action due to the fluid flows in the pipes embedded in the slab. To achieve this objective, a numerical model governing heat conduction is implemented in a computer program in order to calculate and determine the maximum real temperature gradient in the slab based on finite difference calculations that are used to determine the equivalent linear gradient in the slab which will be used for its sizing. The detailed flowchart of this calculation code is shown by Figure 5.

3.3 Description of CTC code

The CTC code is a numerical tool for simulating fluid-structure thermal coupling in order to describe the state of matter throughout the structure based on the explicit finite difference method. The coupling is associated with Gauss and Thomas algorithms for the iterative resolution of the algebraic system [41, 42]. The purpose of the CTC computer program is to characterize

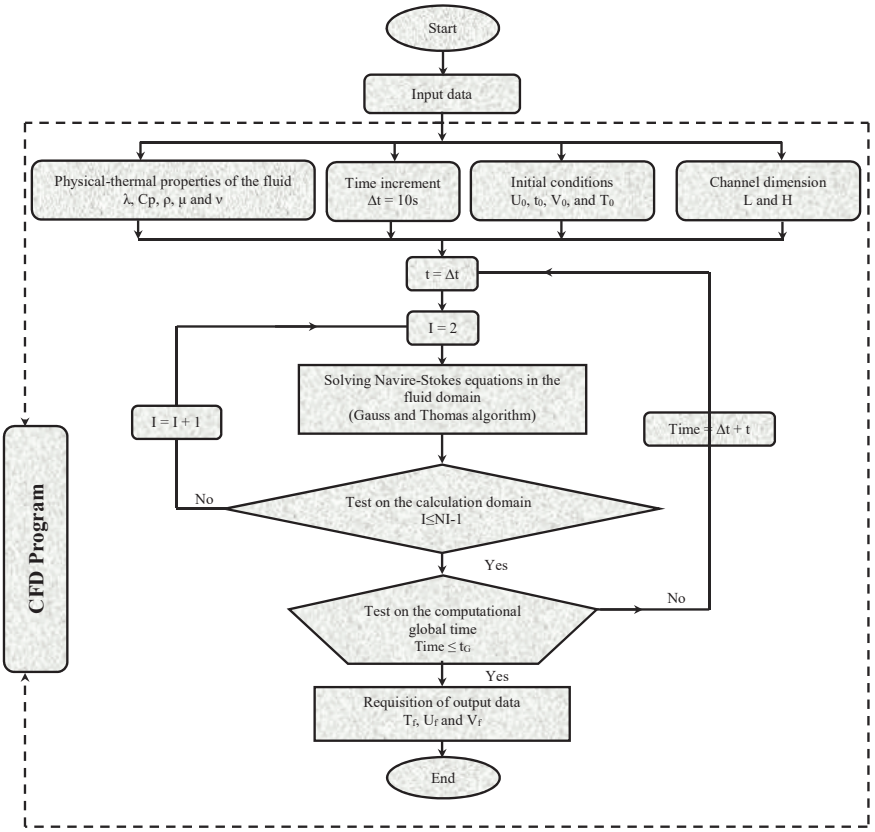

Figure 4 Flowchart of fluid flow modelling in the pipe using CFD code.

the thermal exchange in variable regime between a hot fluid flow in forced convection and a concrete slab, in which the upper face is subjected to ambient temperature. Figure 6 shows the detailed flowchart for this computer code (CTC).

3.4 Description of CTE Code

The CTE calculation code is dedicated to the Modelling of the different transfer modes in the studied habitable envelope and the surrounding atmosphere. In this code, we have implemented a numerical model to describe the exchanges of energy and mass that take place between both media (the atmosphere and the habitat) and which therefore imply their interdependence [43].

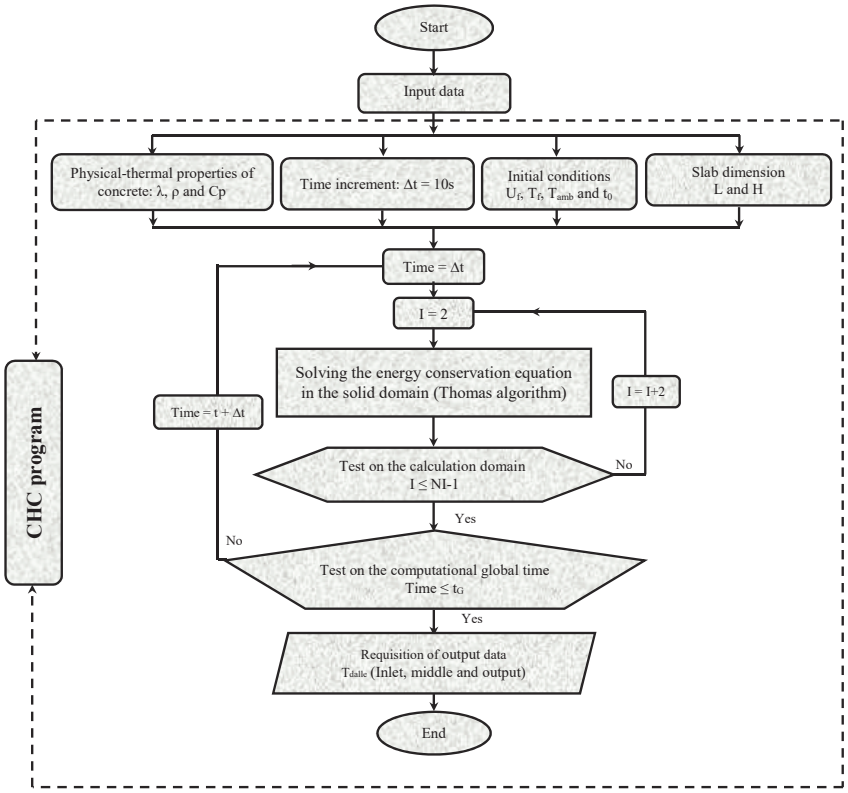

Figure 5 Flowchart of heat conduction modelling in the solid using CHC code.

However, the microclimate affects the internal thermal conditions of the habitat, and consequently its energy behavior in different ways. For this reason, we have taken into account, firstly, the direct and diffuse solar radiations, which are altered by the elements of the habitat and by the building materials and, secondly, the temperature and velocity of the outside air, which influence the conductive and convective exchanges between the habitat and its environment. The effect of conduction in the walls on the interior environment of the habitable envelope and its thermal insulation have also been taken into account [43, 44]. The numerical processing in this computer program was done using the Gauss algorithm [45]. All parts of the habitat are subject to heat transfers, which are heat exchanges between the hot and cold environments (usually from the outside to the inside). The flowchart, in Figure 7, shows the main stages of the heat exchange occurring within the habitable envelope.

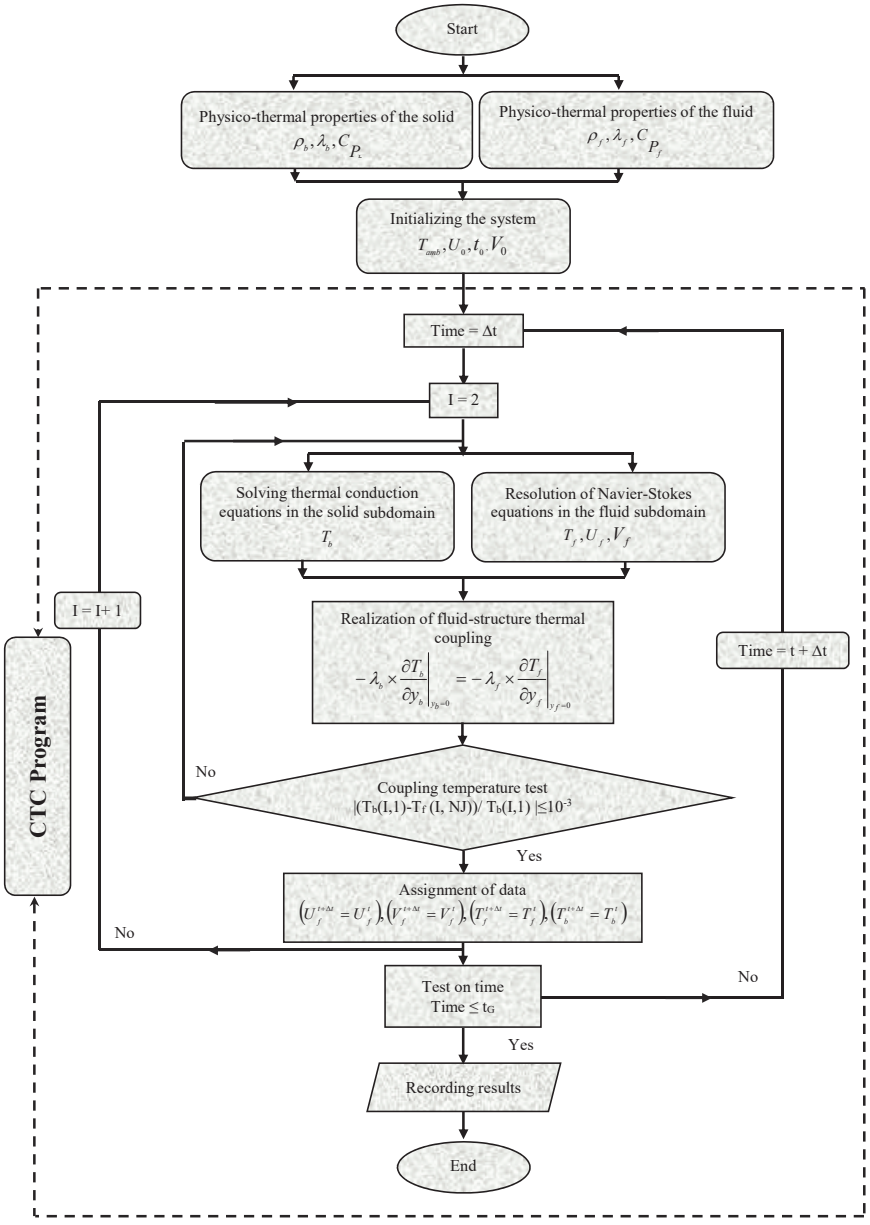

Figure 6 Flowchart of the perfect thermal fluid-structure coupling using CTC code.

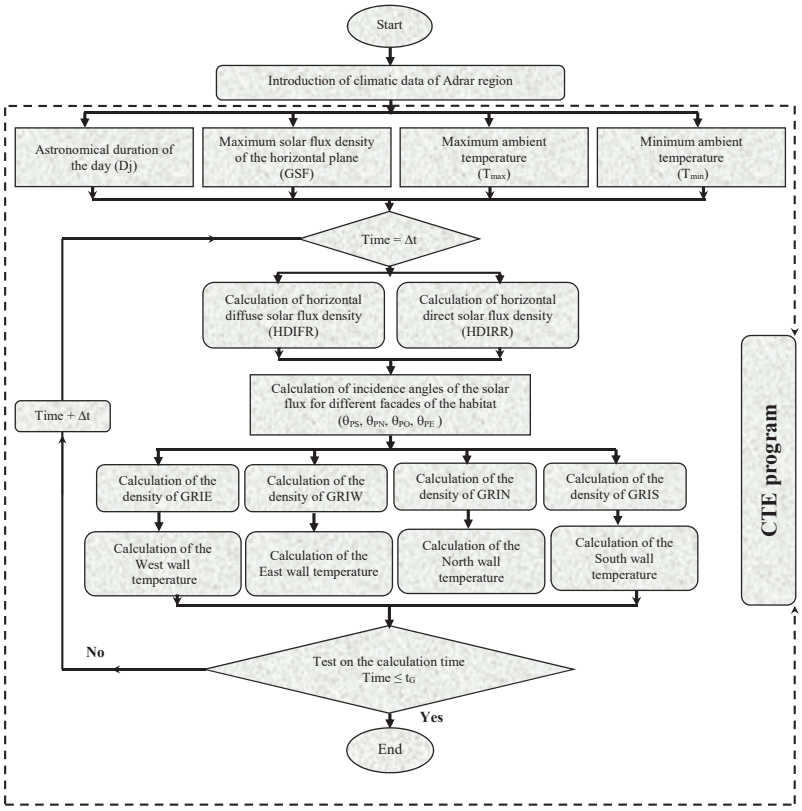

Figure 7 Flowchart of heat exchange modelling in the habitat using CTE code.

3.5 Description of CSR Code

The purpose of the CSR code is to calculate the solar flux values in a typical day. The calculation through this code is based on the assignment of the values of the meteorological variables acquired by the nearest radiometric station [46]. It should be noted that the extraction of the different components of solar radiation from meteorological data depends closely on the exact knowledge of geographical coordinates (latitude, longitude, altitude, etc.) of the position corresponding to the given pixel and the values of the meteorological variables.

The calculation of the solar flux using the CSR code facilitates the optimization of different thermal exchanges within a habitat in order to achieve

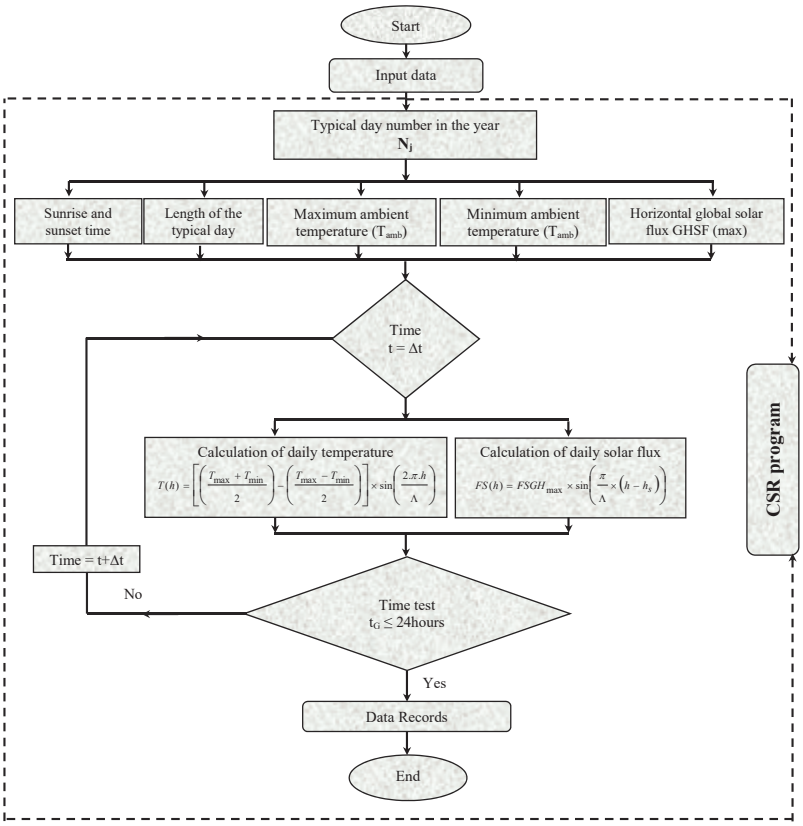

Figure 8 Flowchart of solar radiation modelling using CSR code.

a pleasant and conventional comfort. The detailed flowchart of the CSR calculation code is given by Figure 8.

4 Solving Method

For a time interval $(t_0, t_0 + \Delta t)$, we describe the entire physical system from the first to the last wall. The resolution of the heat balance equations in each wall gives the temperature distribution. The same operations are carried out until the time (t) is completely exhausted. The resulting system of equations is discretized using an implicit finite difference method [47]. This method based on a Taylor series expansion allows to transform these partial derivative equations into a system of algebraic equations, the resolution of which requires

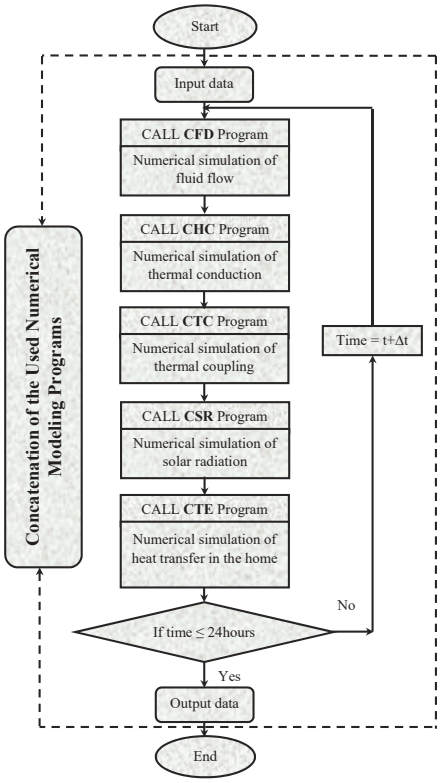

Figure 9 Flowchart illustrating the ordering of the calculation codes developed for the numerical simulation of the different thermal transfer modes.

an iterative calculation to determine the physical quantities at a given time as a function of unknown variables at that same time and known variables at the previous time. At the initial time (t_0), the temperatures of all media are assumed to be equal to the ambient temperature. The flowchart in Figure 9 provides a detailed description of the resolution method adopted in this study.

5 Physical Model

In what follows, we present the main characteristics of the studied habitable envelope. This latter thas a concrete structure of height *'b'*, width 'a' and length *'c'* with opaque walls of thickness *'e'* along the facades (Figure 10-*a*). Internal heating is provided by the floor slab, which consists of three layers comprising a serpentine tube (Figure 10-*b*). The first layer is a thermal

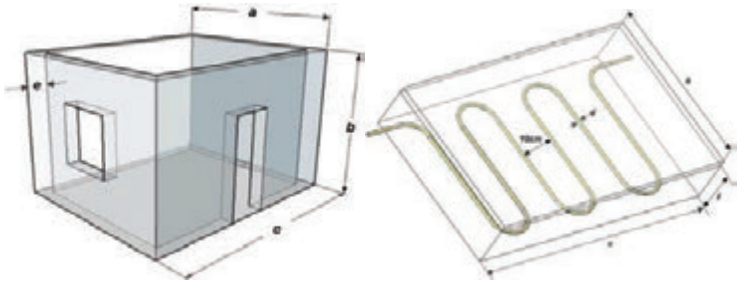

(*a*) The Considered Habitable Envelope. (*b*) The Floor Slab of the Habitat.

Figure 10 Description of the different compartments of the studied physical model.

insulating expanded polystyrene sheet. The height of the layer for insulation is 5 cm. Above it, we have a concrete screed of height *'f'*, length *'c'* and width *'a'*. In the latter are arranged the crosslinked polyethylene tubes which are very often used for the realization of heating floors [48, 49]. Indeed, these semi-rigid pipes are flexible, which are arranged in U-shape with a diameter of 20 mm and a spacing of 10 cm [49]. A concrete covering layer is superimposed on the heating grid. In summer, thermal comfort is provided by opening windows, using blinds and natural ventilation [50].

5.1 Simplifying Assumptions

In this study, we have assumed the following assumptions:

- Transfers are unidirectional;
- The thermal inertia of the air is negligible;
- The air is perfectly transparent to solar radiation;
- The habitat is not a seat of any mass transfer;
- The materials are assimilated to gray bodies;
- The thermophysical properties of materials are constant;
- The celestial vault behaves like a black body;
- The diffuse atmospheric radiation is isotropic;
- The air renewal rate is only considered within the habitat enclosure.

5.2 Physico-Thermal Description of the Studied Habitable Envelope

The habitable envelope simulated in this case study is a mono-zone of 20 m^2 in area and 3 m in height built on flat earth. It is made of molded earth

Table 1 Thermo-physical characteristics of the materials constituting the habitable envelope studied [51, 52]

Walls	Material	$\lambda(W.m^{-1}.k^{-1})$	$\rho(kg.m^{-3})$	$Cp(kJ.kg^{-1}.k^{-1})$	α	ε	$e(cm)$
South wall	Molded earth	1,10	1900	1500	0,80	0,91	20
North wall							
East wall							
West wall							
High floor	Molded earth						
	Palm waste	0,09	350	1000	0,60	0,90	20
Low floor	Full earth	1,10	1900	1500	0,80	0,91	20

Figure 11 Physical aspect of the ancient architecture of the Touat region at Adrar.

bricks, then dried in the sun [51, 52]. The Thermo-physical characteristics are summarized in Table 1:

The earth is arguably the oldest building material, extracted and used locally for millennia, in the form of a mixture of clay, gravel, sand, silt and vegetation [51]. Figure 11 shows the physical aspect of ancient architecture in Touat of the Adrar region (Algeria).

5.3 Choice of the Typical Day

It is possible to determine the monthly typical day (defined by a characteristic declination) and which has a daily irradiation equal to the monthly average. The recommended day for each month with the corresponding day number of the year are given in Table 2. As a result, the monthly averages can be deduced

Table 2 List of typical days per month [54, 55]

N°	Month	Typical Day	Day Number
01	January	17	17
02	February	16	47
03	March	16	75
04	April	15	105
05	May	15	135
06	June	11	162
07	***July***	***17***	***198***
08	August	16	228
09	September	15	258
10	October	15	288
11	November	14	318
12	December	10	344

from the daily sums of extra-terrestrial solar radiation, as follows [53]:

$$\overline{H_0} = H_0|_{\delta=\delta c} \tag{19}$$

Knowing that, the daily amount of extra-terrestrial solar radiation is expressed by:

$$H_0 = \frac{24}{\pi} I_0 \cdot \left(\frac{\pi}{180} \cdot \omega_s \cdot \sin\delta \cdot \sin\varphi + \cos\delta \cos\varphi \cdot \sin\omega_s \right) \tag{20}$$

6 Interpretation of Climatic Data of the Typical Day

In fact, our choice in this case study is based on the notion of the typical day. Based on the climatic data measured by the radiometric station (Figure 12) of the Research Unit for Renewable Energies in the Saharan Environment (URER'MS) of the Touat region of Adrar, we chose July 17th, 2016 as the typical day.

During the crossing of the Earth's atmosphere, solar radiation is divided into several streams due in particular to absorption and scattering processes. Figure 13 show the hourly evolution of solar irradiations in the typical day chosen for the Touat region of Adrar.

Indeed, we note that the evolution of the global solar flux incident on the horizontal plane dominates all the evolutions of other components of the solar flux such as: the direct component and the diffuse component. As we

Figure 12 Photograph of the meteorological station installed at URERMS in Adrar.

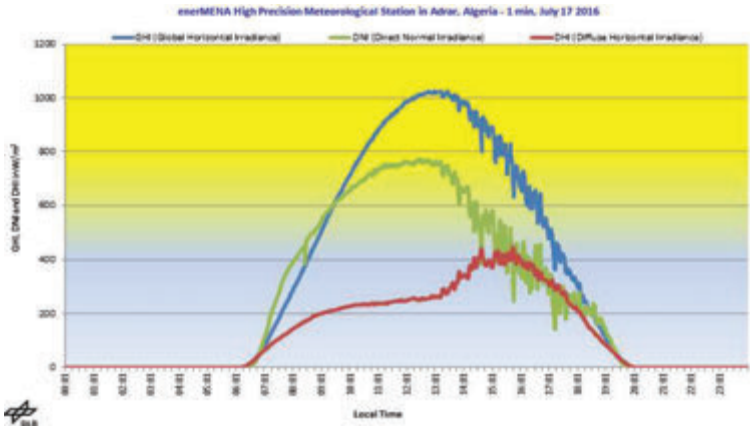

Figure 13 Hourly evolution of solar irradiation on a typical day, July 17th, 2016 for the Touat region of Adrar [56].

have noticed, this evolution is totally linked to the plane orientation and also the course of the sun during the day.

Figure 14 shows the hourly evolution of ambient temperature and relative humidity on a typical day July 17th, 2016 for the Touat region of Adrar. We have noticed through this illustration that the ambient temperature and the relative humidity are visibly constant throughout the day whose values are respectively 35.3°C and 11.9% for relative humidity.

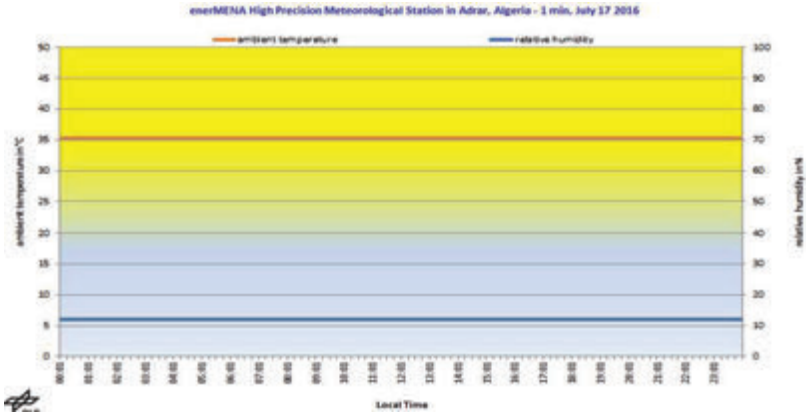

Figure 14 Hourly evolution of ambient temperature and relative humidity on a typical day July 17th, 2016 for the Touat region of Adrar [56].

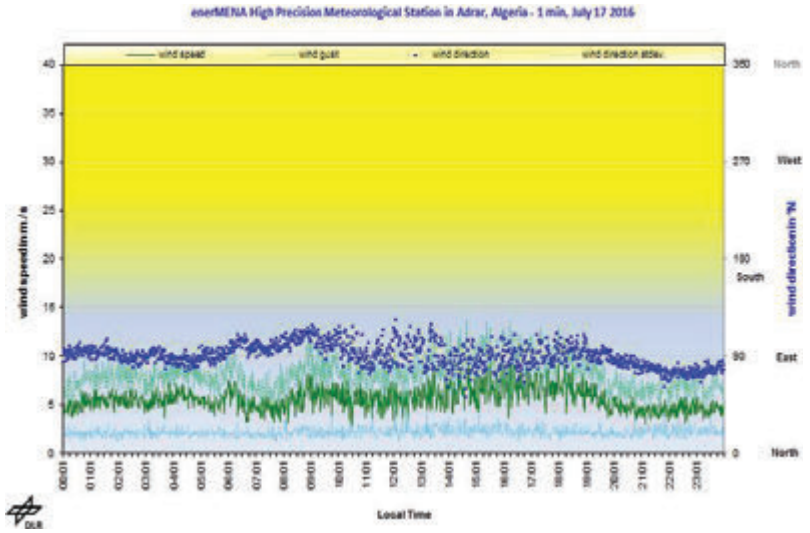

Figure 15 Hourly evolution of the average wind speed on a typical day July 17th, 2016 for the Touat region of Adrar [56].

Figure 15 show the monthly average distribution of wind speed of the typical day July 17th, 2016 at the Touat site measured by the URER'MS radiometric station of Adrar at a height of 10 m from the ground. It can be seen that this day is characterized by considerable hourly variations. Knowing that, this variation reaches its maximum value around 13.3 m/s

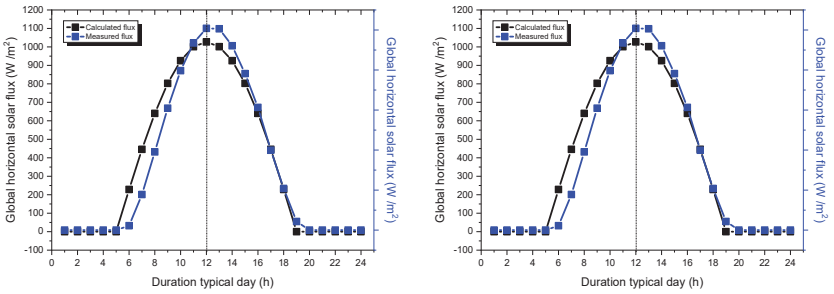

(a) (b)

Figure 16 Comparison between the calculated and measured values of (a) the horizontal global solar flux and (b) the horizontal direct flux in a typical day as a function of the local time.

around 12:01 am in local time with an average speed of 9.6 m/s during the period from 09h30 am to 10h30 am.

7 Results and Discussion

7.1 Validation

Figure 16 show a comparison between the calculated and measured values of the global horizontal solar flux and the direct horizontal flux as a function of the local time of the typical day considered. It is found that there is an acceptable agreement between the results obtained by the developed model and those measured by the URER'MS radiometric station of Adrar, with relative errors equal to 1.44% for the global flux and 1.25% for the direct horizontal flux.

7.2 Positioning of the Sun in a Typical Day

The accurate positioning of the sun in the sky at a given time is determined by means of three fundamental quantities such as: The azimuth of the sun, the sun angular height and the sun hourly angle. Indeed, the sun angular height varies between 0° in the night period and 90° at solar noon as shown in Figure 17(a). Moreover, the sun azimuth is negative before solar noon, positive in the afternoon and zero at solar noon as shown in Figure 17(b). In addition, the hourly angle of the sun is the parameter that identifies the sun position on its diurnal trajectory and is directly related to the date, time and meridian of the observation location. The hourly angle is determined by

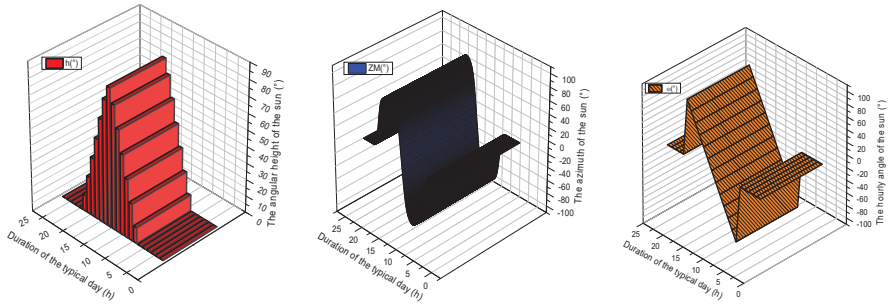

(a) (b) (c)

Figure 17 Evolution of (a) the sun angular height, (b) the sun azimuth and (c) the sun hourly angle as a function of the local time of a typical day.

setting as a reference (0° for the solar noon (12h), −90° for 6h solar and +90° for 18 h solar) (see Figure 17(c)).

7.3 Evolution of the Concrete Slab Temperature

Figure 18 shows the variation of the heating slab temperature as a function of the space step ratio for four different times and at three different positions in the system (at the inlet, middle and outlet). We can notice that:

- The evolution of thermal diffusion in the concrete slab is almost similar for the three considered positions (inlet, middle and outlet);
- There is a noticeable difference in temperature between the positions in the system for the four selected global calculation times;
- For a space step ratio varying between 0 and 0.12 and with a fluid inlet temperature of 60°C at the middle, the heat propagation in the solid decreases up to temperature values around 38°C for t = 3600 s (Figure 15(a)), 47°C for t = 10800 s (Figure 15(b)), 48°C for t = 14400 s (Figure 15(c)) and 49°C for t = 43200 s (Figure 15(d)).

7.4 Evaluation of Solar Fluxes of the Habitable Envelope

Figure 19 show the presentation of the components (direct and diffuse) of the horizontal global solar flux density (GSF) in true solar time for the typical day considered. Indeed, for a perfectly sunny day and in the absence of any reflecting surface, it can be seen that the values illustrated in Figure 15 are only meaningful in terms of the instantaneous power of the hourly solar flux density. It is also noted that for all the values of the global solar flux density

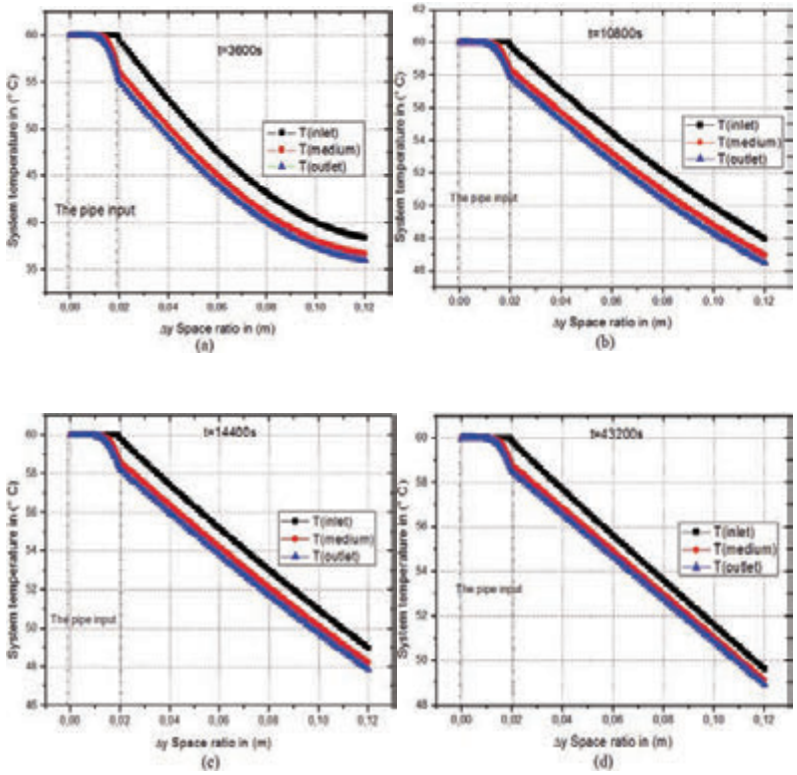

Figure 18 Comparison between the three profiles (inlet, middle and outlet) of the temperature as a function of the space step ratio of the slab for: (a) t = 3600s, (b) t = 10800s, (c) t = 14400s and (d) t = 43200s.

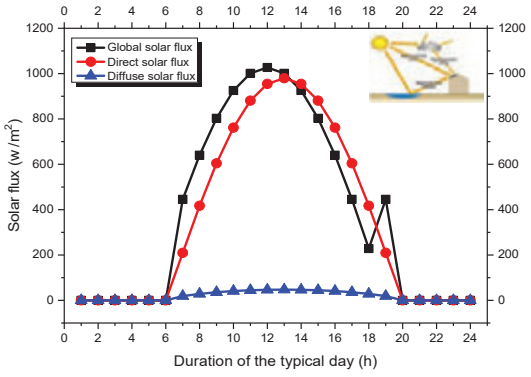

Figure 19 Evolution of the global (GSF), direct (HDIRR) and diffused (HDIFR) horizontal solar flux profiles for a typical day as a function of local time.

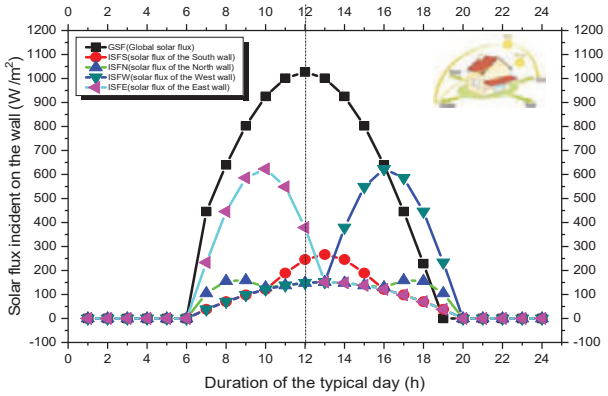

Figure 20 Evolution of the incident solar flux profiles on the different facades of the habitat as a function of the local time of the typical day.

received by a horizontal plane in a typical day, there must be on the one hand a component of the direct solar flux density (HDIRR) which has slightly smaller values compared to those of the global flux. On the other hand, another component of diffuse solar flux density (HDIFR) with values also smaller than those of direct solar flux density. In addition, a slight increase was noted for the streamflux between 06 am and 08 pm.

Figure 20 show the comparison of the hourly evolution of the density of the incident solar flux on the different facades of the habitat (Roof, South, East, West and North) during the typical day considered. Indeed, according to this comparative representation between the different facades of the habitat, it can be observed that the totality of the densities of the solar flux for the East, West, North and South facades have lower values than those of the incident flux on the roof of the habitat because physically, the horizontal facade (roof) with an inclination angle of 0° receives more solar flux compared to other vertical facades with an angle of 90°.

7.5 Thermal Exchange of the Habitat Facades

On the basis of the climatic data measured by the radiometric station of the URER'MS of ADRAR, Figure 21 presents a comparison between the temperatures of the external facades of the habitat, calculated by the numerical model developed for the selected typical day. According to this figure, it can be seen that the temperatures describing the thermal exchange between the external facades of the east walls (TEFE) and the roof of the habitable envelope (TEFCS) have a maximum value of 42°C, which is recorded at

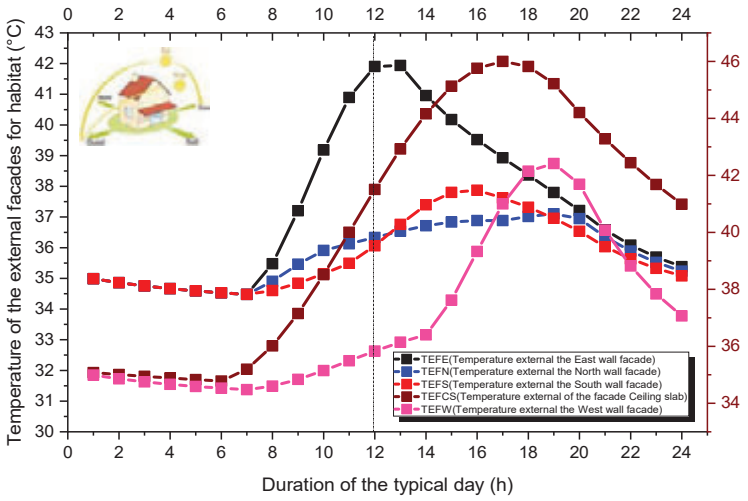

Figure 21 Evolution of the habitat external facades temperatures as a function of the local time in a typical day.

noon for the east wall and at 06 pm for the habitat roof. These temperatures were recorded with a time phase shift equal to 05 hours. In addition, we noted that the maximum value of temperature of the west facade is 38.5°C recorded at 06 pm, while those of the north and south facades are 37.5°C recorded at 03 pm. On the other hand, we noticed a notable phase shift between the maximum temperature of the north, south and west facades equal to 03 hours. In conclusion, this phase shift, between the optimal temperature of the external facades of the habitat amounts to the course of the sun during the typical day of the year considered.

Figure 22 show the hourly temperature variation of the different internal facades as well as the temperature of the internal space of the habitable envelope during the typical day. It is found that the low thermal inertia of the clay plays a very important role in the thermal exchanges at the level of the habitat walls. To this end, the internal facade temperature from the ceiling floor (TIFCS) is decreasing from 35.5°C to 32°C, knowing that this facade receives the greatest amount of solar flux during the full day in comparison with the other facades of the habitat. On the other hand, we notice that the evolution of the temperature of the internal south facades (TIFS) and internal north facades (TIFN) have the same variation trend with a decrease of 39°C to 31°C during the period from 1 h to 24 h (00 h). Also, we noticed that the temperatures of the west facade (TIFW), the bottom ceiling facade (TIFCS)

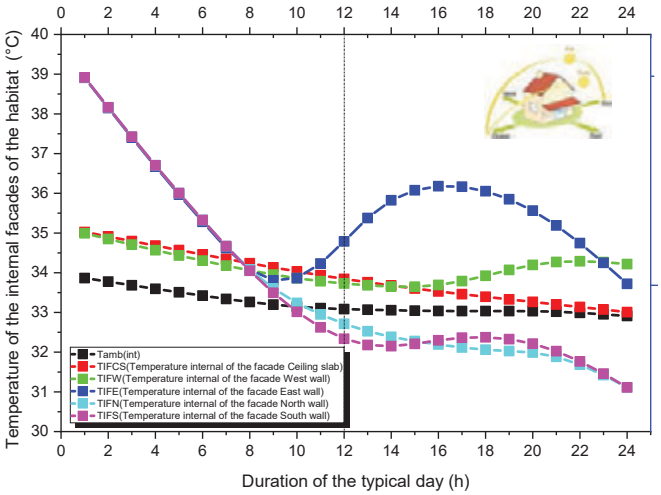

Figure 22 Evolution of the temperature of the habitat internal facades as a function of the local time in a typical day.

and the internal space (T_{amb}) have almost the same evolution during the whole day with a maximum temperature of 35.5°C at 01 am and 33°C at 00h00. In addition, a significant value was recorded for the temperature of the internal east facade (TIFE) of 36°C to 04 pm in the afternoon.

7.6 Evolution of Dimensionless Numbers of Heat Transfer

Figure 23 show the evolution of the two dimensionless numbers of Nusselte (Nu) and Grashof (Gr) as a function of the typical day duration. According to this figure, it can be seen that the evolution profiles of Nu and Gr have an increasing trend. Indeed, this growth in the two dimensionless numbers Nu and Gr started from 03 am. However, the increase in the Nu number, reflects the importance of the contribution of the ambient air flux on the heat exchange with the wall of the bottom ceiling of the habitat (WBC). On the other hand, the increase in the Gr number, reflects an increase in the intensity of the natural convection within the habitable envelope.

7.7 Comparative Study According to the Thermal Comfort

Figure 24 show a comparison between the thermal comfort temperature and the internal space temperature of the habitat during a typical day. It can

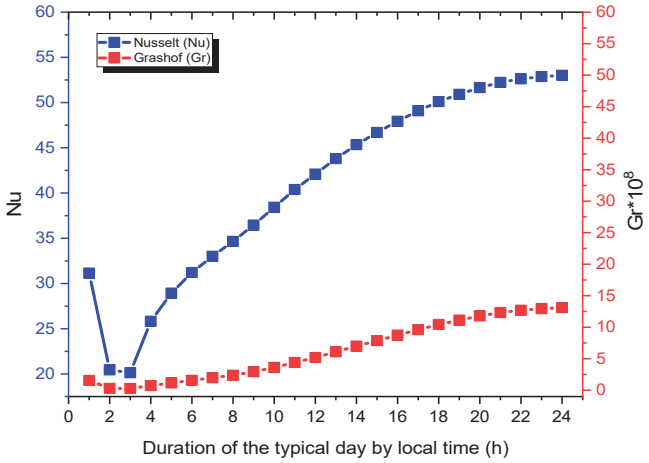

Figure 23 Evolution of the Nusselt and Grashof numbers as a function of the local time in a typical day.

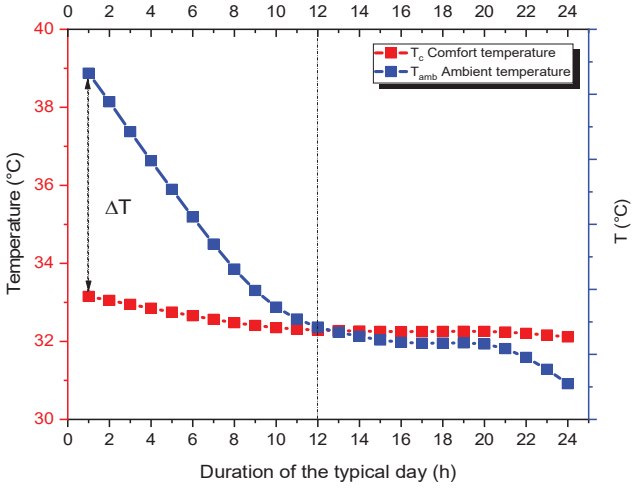

Figure 24 Comparison between the comfort temperature and the internal space temperature of the habitat during the typical day.

be seen that the evolution of the internal space temperature of the habitat decreases from 01h00 am with a temperature of 39°C until the end of the day with a temperature of 31°C. In addition, we also notice that the evolution of the thermal comfort temperature is almost stable with an average comfort temperature of 32.5°C during the whole day. On the other hand, it is well

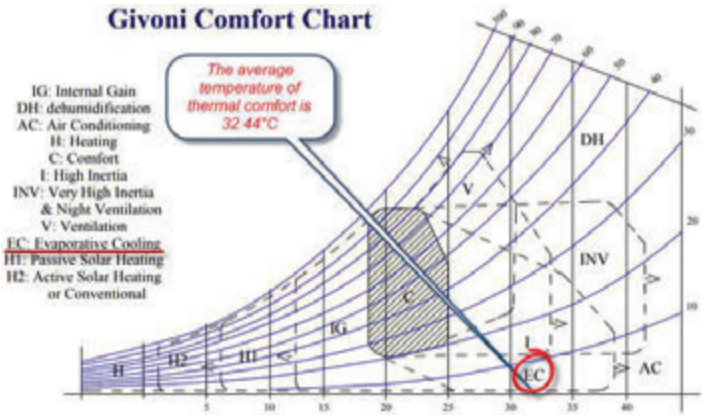

Figure 25 Determination of the thermal comfort temperature using Givoni psychometric diagram.

observed that there is a gap of 6°C between the thermal comfort temperature and the internal ambient temperature. It should be noted that from solar noon, the temperature of the internal ambient began to stabilize until 8:00 pm and then it decreases rapidly until the end of the day. This degradation in the ambient temperature of the habitable envelope is an advantage due to the physico-thermal properties of the clay used as a building material in these severe conditions of ADRAR region.

Figure 25 show the position on the Givoni diagram of the thermal comfort temperature calculated using a mathematical model. The location of the thermal comfort temperature on this diagram, allows us to evaluate and find the technical-thermal solutions in order to check the conventional standards of comfort in the habitat. However, we found that the positioning of the comfort temperature of 32.44°C on the Givoni diagram is in zone (I), which is the thermal inertia zone of the construction material. This area requires a technical-thermal solution such as evaporative cooling.

8 Conclusion

The research carried out in this paper has two main objectives: The first is to develop a computer tool for numerical simulation of thermal exchanges in buildings. The second is devoted to the estimation of the amount of solar flux incident on the different facades of a habitat based on real measured climatic data in order to optimise thermal comfort. The case study that was

presented using the developed calculation programs showed that it is possible to highlight the instantaneous evolutions of the different components of the incident solar flux on a surface with any orientation and inclination. From the results presented above, the following conclusions can be drawn:

- The comparison of the values estimated by the developed models and the measured values provided by (URER'MS) of Adrar Radiometric Station proves to be acceptable on the whole.
- It is important to know the position of the sun in the sky, the magnitude of the solar flux contributions of the habitable envelope and their influences on the temperature evolution of different internal and external facades of the walls during the typical day.
- The increase of the Nusselte number (Nu) is greater than that of Grashof (Gr), which reflects the importance of the ambient air flow contribution on the heat exchange with the ceiling bottom wall of the habitat compared to the contribution of the natural convection within the habitable envelope.
- From the comparative study with respect to thermal comfort, we found that the reconciliation between the two values of internal space temperature and thermal comfort took place from solar noon.

Finally, we can say that these computational codes can then be coupled to a professional and user-friendly interface so that it can be easily used by specialists in this field and work on this way is under investigation.

Acknowledgments

The authors would like to acknowledge the General Directorate of Scientific Research and Technological Development (DGRSDT) of Algeria, LABAB Laboratory of National Polytechnic School of Oran and LDDI Laboratory of Ahmed Draya University of Adrar for research grants and funding as welle as the URER'MS for the provision of climate data.

References

[1] M.R. Yaïche et S.M.A. Bekkouche, Conception et validation d'un programme sous Excel pour l'estimation du rayonnement solaire incident en Algérie. Cas d'un ciel totalement clair, Revue des Energies Renouvelables Vol. 11 N°3 (2008) 423–436.

[2] F. Yettou, A. Malek, M. Haddadi et A. Gama, Etude comparative de deux modèles de calcul du rayonnement solaire par ciel clair en Algérie, Revue des Energies Renouvelables Vol. 12 N°2 (2009) 331–346.

[3] N. Zarai, M. Chaabane and S. Gabsi, Outil de planification de la production thermique des capteurs solaires, International Renewable Energy Congress, November 5–7, 2010 – Sousse, Tunisia, ID155.

[4] Z. QU, La nouvelle méthode Heliosat-4 pour l'évaluation du rayonnement solaire au sol, Thèse de doctorat de l'école nationale supérieure des mines de Paris, 2013.

[5] A. Raad, Co-simulation et optimisation multi-critères en conception de bâtiment, par approche d'interopérabilité de services, Thèse de doctorat l'université de Grenoble Alpes, France, 2017.

[6] L. Arantes, S. Marry, O. Baverel et D. Quenard, Efficacité énergétique et formes urbaines: élaboration d'un outil d'optimisation morpho-énergétique, Cybergeo: European Journal of Geography, Aménagement, Urbanisme, document 777, mis en ligne le 07 avril 2016, doi: 10.4000/cybergeo.27584.

[7] V. B. Dinh, B. Delinchant, F. Wurtz, Dimensionnement optimal des systèmes énergétiques intégrant la stratégie de gestion pour une maison raccordée au réseau, Symposium de Genie Electrique, Jun 2016, Grenoble, France, hal-01361643.

[8] A. Jean, Contribution à l'Étude des Parois Complexes Végétalisées (PCV): Évaluation de la Performance Énergétique Globale en Climat Tropical Humide, Thèse de doctorat de l'université de La Réunion, la France, 2015, tel-01724632.

[9] A. Oudrane, B. Aour, M. Hamouda et M. Benhamou, Méthodologie pour la détermination de l'écartement optimal de la chaîne tubulaire d'une dalle chauffante, Revue des Energies Renouvelables Vol. 19 N°1 (2016) 11–19.

[10] E. Noel, M. Delaune (2012), Simulation numérique des équations de Navier-Stokes, Projet de Physique P6-3 STPI/P6-3/2011–39, institut national des sciences appliquées de Rouen département sciences et techniques pour l'Ingénieur, de l'université -76801 Saint Etienne du Rouvray.

[11] P. Marty (2012), Transferts thermiques convectifs, Génie des Procédés Master 2, Université Joseph Fourier, Grenoble, la France.

[12] N. B. Hassine, X. Chesneau, A. H. Laatar (2017). Numerical simulation of heat and mass transfers during solar drying of sewage sludge: Radiation effect, Energy Procedia 139, pp. 804–809.

[13] M. S. Abdul Aziz, M. Z. Abdullah (2014). Thermal Fluid-Structure Interaction in the Effects of PinThrough-Hole Diameter during Wave Soldering, Hindawi Publishing Corporation Advances in Mechanical Engineering Volume 2014, Article ID 275735, 13 pages, doi.org/10.1 155/2014/275735.

[14] A. Oudrane, B. Aour, M. Hamouda et M. Benhamou, Méthodologie pour la détermination de l'écartement optimal de la chaîne tubulaire d'une dalle chauffante, Revue des Energies Renouvelables Vol. 19 N°1, pp. 11–19, 2016.

[15] Y. Debard, Méthode des éléments finis: thermique, Master Modélisation Numérique et Réalité Virtuelle, Université du Mans, 29 mars 2011.

[16] A. D. Chiasson, J. D. Spitler, S. J. Rees, A Model for simulating the performance of a pavement heating system as a supplemental heat rejecter with closed-loop ground-source heat pump systems, Journal of Solar Energy Engineering, Vol. 122, (2000), 183–191.

[17] M. P. Errera, G. Chaineray, S. Chemin (2007). "Etude du transitoire thermique dans un matériau via un couplage convection-conduction". Congrès Français de Thermique, SFT 2007, Île des Embiez.

[18] E. Saatdjian (1998). "Phénomènes de transport et leurs résolutions numériques". 2éme édition, Polytechnica, 15 rue Lacépède F-75005, ISBN2-84045-057-6, Paris.

[19] G. Florides, S. Kalogirou (2007). "Ground heat exchangers – A review of systems: models and applications". Renewable Energy 32, pp. 2461–2478.

[20] M. Ghalambaz, E. Jamesahar, A. Ismael, J. Chamkha (2017). "Fluid-structure interaction study of natural convection heat transfer over a flexible oscillating fin in a square cavity". International Journal of Thermal Sciences 111, pp. 256–273.

[21] A. Al-Amiri, K. Khanafer, Fluid–structure interaction analysis of mixed convection heat transfer in a lid-driven cavity with a flexible bottom wall, International Journal of Heat and Mass Transfer 54 (2011) 3826–3836.

[22] S. Mergui, Transferts thermiques, licence de mécanique 2éme année, UPMC, université de Sorbonne.

[23] S. Abide, S. Viazzo, C. Solliec, Simulation numérique du refroidissement d'une plaque plane par un jet plan impactant, LAMPS-GME, Université de Perpignan, 52 Avenue Paul Alduy, 66860 Perpignan, la France. https://docplayer.fr/25679830-Simulation-numerique-durefro

idissement-d-une-plaque-plane-par-un-jet-planimpactant.html, (Page consulté le 29/05/2018).

[24] D. Gobin, D. Levesque, C. Benard, Stockage de l'énergie solaire: simulation numérique du transfert d'énergie par conduction et rayonnement dans un milieu à deux phases, revue de physique appliquée, tome 14, page 125, janvier 1979.

[25] A. Compaore, B. Dianda, G.t Nana, D. Joseph Bathiebo, B. Zeghmati, X. Chesneau and S. Abide, "Modelling of Heat Transfer in a Habitat Built in Local Materials in Dry Tropical Climat", Physical Science International Journal, 17(1): pp. 1–11, 2018.

[26] H. Wang, S. Xin, P. Le Quéré, "Étude numérique du couplage de la convection naturelle avec le rayonnement de surfaces en cavité carrée remplie d'air". C.R. Mécanique 334 (2006), pp. 48–57. doi.org/10.1016/j.crme.2005.10.011.

[27] A. Oudrane, B. Aour, B. Zeghmati, X. Chesneau, M. Hamouda, "Analysis numerical of onedimensional heat transfer for desert house ", Recueil of mécanique, Vol. 2 n°01, (2017), 089–102. doi: 10.5281/zenodo.1134955.

[28] G. Flamant et G. Arnaud, "Analyse et modélisation du transfert de chaleur entre une paroi et un lit fluidisé haute température", hf. J. Heat Maw Transfer. Vol. 27, No. 10(1984). pp. 1725–1735. doi.org/10.1016/0017-9310(84)90155-8.

[29] M. Gacem, Comparaison entre l'isolation thermique extérieure et intérieure d'une pièce d'un habitat situé dans le site de Ghardaïa, Thèse de magister de l'université de Abou-Bekr Belkaid-Tlemcen, 2011.

[30] P. Severin, Traitement des ambiances: Applications à l'habitat et aux locaux professionnels de l'hôtellerie – Restauration, Sciences et Technologie de l'Habitat et de l'Environnement, IUFM de Toulouse Biotechnologie B.

[31] A. Oudrane, Aour B., Belkacem Z., Xavier C., Hamouda M. "Parametric Optimization of Thermal Comfort in Extreme Weather Conditions". International Journal of Engineering Research in Africa, Vol. 44 (2018), pp. 75–90. doi:10.4028/www.scientific.net/JERA.44.75.

[32] B. Bouchekima, B. Gros, R. Ouahes, M. Diboun, "Etude théorique et application pratique du distillateur solaire à film capillaire", Int. J. Therm. Sci. (2000) 39, pp. 442–459. doi.org/10.1016/S1290-0729(00)00216-7.

[33] S.A. Klein, Calculation of monthly average insolation on a tilted surface, Solar Energy, (1977) 325–329.

[34] P. M. Collares, et A. Rabl, The average distribution of solar radiation between daily and hourly values, Solar Energy, (1979) 155–164.
[35] L. Yuehua, J. Yingni, C. Xinxiao, "Evaluation of three models for calculating daily global solar radiation at Yushu, Tibet", IEEE International Conference on Consumer Electronics, Communications and Networks (CECNet), pp. 1252–1255, 2011.
[36] A. Kaddour, Modelisation et simulation d'un concentrateur parabolique solaire a moteur Stirling en vue d'un rendement optimal, PhD Thesis, University of Abou Bekr Belkaid, 2013.
[37] Y. El Mghouchi, A. El Bouardi, Z. Choulli, T.Ajzoul "New model to estimate and evaluate the solar radiation", International Journal of Sustainable Built Environment, Vol. 3, No. 2, pp. 225–234, 2014.
[38] N. B. Hassine, X. Chesneau, A. H. Laatar, Numerical simulation of heat and mass transfers during solar drying of sewage sludge: solar radiation effect. International Conference On Materials And Energy 2015, ICOME 15, 19–22 May 2015, Tetouan, Morocco, and the International Conference On Materials And Energy 2016, ICOME 16, 17–20 May 2016, La Rochelle, France, Energy Procedia 139 (2017) 804–809.
[39] A. Oudrane, B. Aour, Numerical investigation of a laminar flow in a tubular chain of a heated floor slab, Recueil de mécanique vol. 2 n°002 (2017) 192–203.
[40] A. Oudrane, B. Aour and M. Hamouda, Numerical investigation of thermal exchanges for a habitab l'enclosure in a desert region, International Journal of Renewable Energy, Vol. 12, No. 2, July – December (2017) 87–105.
[41] T. Heuzé, J. B. Leblond et J. M. Bergheau, Modélisation des couplages fluide/solide dans les procédés d'assemblage à haute température, Mécanique et Industries 12, 183–191 (2011), doi: 10.1051/meca/2011113.
[42] E. Mladin, M. Lachi et J. Padet, Transfert de chaleur couplé conduction-convection en régime instationnaire, induit par une température imposée sur une plaque d'épaisseur finie, Congrès Français de thermique, SFT2001, Nantes, 29–31 mais 2001.
[43] N. D. Pellegrin, Modélisation fine des échanges thermiques entre les bâtiments et l'atmosphère urbaine, Thèse de doctorat de l'université de Paris-EST, France, 2016.
[44] F. Mokhtari1, N. Ait Messaoudéne, A. Hamid et M. Belhamel, Etude du comportement thermique d'une maison munie d'un système de

chauffage solaire, 12èmes Journées Internationales de Thermique, Tanger, Maroc du 15 au 17 Novembre 2005.

[45] C. Yacouba, Etude numérique des performances thermiques d'un habitat bioclimatique, Thèse de doctorat de l'université de Perpignan Via Domitia de l'unité de recherche: LAMPS – EA UPVD 4217, France, 2018.

[46] F. Lantri, N.I. Bachari et H. Belbachir, Estimation et cartographie des différentes composantes de rayonnement solaire au sol à partir des données météorologiques, Revue des Energies Renouvelables Vol. 20 N°1 (2017) 111–130.

[47] M. Rachid Laydi, "Une méthode nodale à deux niveaux pour la résolution du problème de Stokes", C. R. Acad. Sci. Paris, t. 324, Serie 1(1997), pp. 1075–1078. doi.org/10.1016/S0764-4442(97)87889-5.

[48] Fiche Technique Tube PER Prégainé, 91, Rue Duruisseau, PA des Chesnes – 38297 St Quentin – Fallavier, Date de mise à jour: 22/06/2016.

[49] A. Oudrane, B. Aour, M. Benhamou, Étude et analyse paramétrique d'une installation solaire: plancher solaire dicte d'implanter dans la région d'Adrar, ElWahat pour les Recherches et les Etudes Vol. 9 n°1, pp. 27–49, 2016.

[50] B. Moujalled, Modélisation dynamique du confort thermique dans les bâtiments naturellement ventilés, Thèse de doctorat de L'école centrale de Lyon, laboratoire de tribologie et dynamique des systêmes, Bât. G8, 36 avenue Guy de Collongue, BP 163, 69131 Ecully Cedex, la France, 2007.

[51] Réglementations Thermique acoustique aération des bâtiments d'habitation neufs dans les DOM, Fiche d'application – Thermique – Protection contre les rayonnements solaires, Ministère de l'écologie, du développement durable et de l'énergie, 2011.

[52] C. Lnard, P. Depecker, J.-J. Roux, "Un modéle simplifié pour la prédiction du champ de température dans les bâtiments", Rev Gén Therm (1997) 36, pp. 113–123. doi.org/10.1016/S0035-3159(99)80056-7.

[53] K. Bouchouicha, Modélisation multi spectrale des images satellitaire – Application: quantification du bilan d'énergie sol-atmosphère, Thèse de doctorat de l'université de sciences et technologie d'Oran (USTO), 2017.

[54] ISO-9060 Standard et Pyranometer Measurement Accuracy (2014). Consulté 09/08/2019. http://ases.conferenceservices.net/resources/252/2859/pres/SOLAR2012_0829_presentation.pdf.
[55] K. Mansatiansin, Modélisation et simulation des transferts et de l'éclairement dans un habitat bioclimatique, thèse de doctorat en sciences de l'ingénieur, spécialité mécanique énergétique, université de Perpignan, 2005.
[56] Technical Report, EnerMENA High Precision Meteorological Station of Research Unit for Renewable Energies in the Saharan Environment, in Adrar, Algeria, 2016.

Biographies

Abdellatif Oudrane has been working at the Faculty of Science and Technology at ADRAR's Ahmed Draïa University since September 2019. He has conducted research in the fields of solar thermal, environment and renewable energies. Its largest objective is the detailed theoretical and practical study of exchanges (radiative, conductive and convective) at the level of all building components. His studies are based on the thermo-physical and dynamic characterization of ambient air.

Benaoumeur Aour was born in 1970 in Algeria. He took the diploma of Habilitation (Post-Doc) in Mechanical Engineering at the University of Oran (Algeria) in 2008. He obtained the rank of Professor in January 2014. His main areas of research are centered on numerical methods for the calculation of structures, the mechanics of materials and biomechanics. He has published in several national and international journals. He has also contributed to the expertise of several scientific research works (doctoral theses, scientific books, publications, communications, etc.) He is currently the director of the Laboratory of Applied Biomechanics and Biomaterials (ENP Oran) and chief of several projects on mechanics and biomechanics.

Messaoud Hamouda is Professor at the University of Adrar. He received his diploma of Engineer and Magister in electrical engineering from The University of Sciences and Technology of Oran (USTO), Algeria, respectively in 1992 and in 1997. He obtained his Phd degree in electrotechnics in 2007 from The University of Sciences and Technology of Oran. Within the Unit of Renewable Energy Research in Saharan medium of Adrar, he has been managing director for seven years. Currently, he is a Director of Laboratory of Sustainable Development and Informatics.